Structure of interfacial liquids: X-ray scattering studies

C.-J. Yu, A. G. Richter, J. Kmetko, S. W. Dugan, A. Datta, and P. Dutta
Department of Physics and Astronomy, Northwestern University, Evanston, Illinois 60208-3112
(Received 10 July 2000; published 25 January 2001)

We have used synchrotron x rays to study three different liquids near solid-liquid interfaces. For either ultrathin (45–90 Å) or thick (~5000 Å) liquid films on silicon substrates, we find (on the basis of diffraction peaks or specular reflectivity data) that the molecules form 3–6 layers at the interface, with plane spacings close to the molecular dimensions. Rough surfaces and/or impurities reduce the density oscillation amplitudes. Making the liquid film very thin does not observably enhance the effect, which implies that layering is present even at an isolated interface (i.e., in a semi-infinite liquid). On the other hand, predeposited impurities diffuse away from the interface more easily if the liquid films are thick. The liquids studied are nonconducting, nonpolar, and nonreactive; the molecules are roughly spherical; and our substrate surface has no lateral structure. Thus our observations should apply to any liquid near a hard wall.

DOI: 10.1103/PhysRevE.63.021205 PACS number(s): 61.20.−p, 68.08.−p, 68.15.+e

I. INTRODUCTION

The behavior of liquid molecules at solid-liquid interfaces is relevant to a variety of static and dynamic processes, including adhesion, wetting and spreading, lubrication, many chemical reactions, thin film growth, coating technology, etc. [1]. However, such internal interfaces are not easily accessible to many experimental probes. This article describes our x-ray scattering studies of ordering in normal (nonmetallic, non-liquid-crystalline, nonreactive, nonpolar) liquids of roughly spherical, nonentangling molecules, near solid–liquid interfaces.

A number of experiments [1–13] show clearly that the physical properties of interfacial liquids cannot be understood on the basis of continuum hydrodynamics. Surface force measurements between two mica plates immersed in liquid show that the force is not monotonic, but contains oscillations as a function of plate separation, attributed to ''structural forces'' not contained in van der Waals based models [2]. The period of the oscillation corresponds to one of the dimensions of the liquid molecule. Ellipsometric observations of stepwise spreading [3] and thickness-dependent variations in the evaporation rate [4] provide other evidence of this periodicity. The viscosity of a liquid film can be at least 10^7 times that of the same liquid in bulk if the film thickness is less than 6 to 7 times the molecular dimensions [5]. The observation of stick-slip motion during lateral translation of the plates confining the thin film provides dynamical evidence of lateral ordering [6]. These experiments, however, do not show the internal structure directly.

The use of strong, highly collimated x-ray beams from synchrotrons, at grazing incident angles, allows the determination of structure in the small amounts of material at or near surfaces and interfaces. X-ray studies of liquid metals have shown that there is layering at the free surface [9,10]. Either because of the narrow interface width (<1 Å) caused by the large surface tensions of liquid metals, and/or because of the sharp boundary that must exist between the electronic structure of the liquid and that of the vapor [14], there is a relatively smooth ''hard wall'' at the free surfaces of liquid metals. No evidence of layering has ever been observed at the free surfaces of insulating fluids, which are much less sharp.

However, even an insulating liquid encounters a hard wall at a solid-liquid interface. Looking at the structure of the interfacial liquid with x rays requires the photons to penetrate either the liquid or the solid, which results in attenuation of the main beam and a larger background due to scattering from material that is not of interest. While this increases the degree of difficulty, it is still possible to obtain useful data, as we shall show.

Prior to our own work, there has been only a single scattering experiment reporting non-liquid-like structure in a liquid near a liquid-solid interface. Huisman *et al.* [11] have studied the structure of gallium at a diamond-gallium interface by sending x rays through a diamond crystal. The ultrapure liquid gallium was introduced in a UHV chamber onto a nonreactive (2×1) reconstructed diamond (111) surface. Gallium does not wet diamond (contact angle ~116°), and thus only a macroscopic amount of liquid can be deposited. This would lead to unacceptably large diffuse scattering if x rays were sent through the disordered liquid; therefore the x rays were sent through the ordered diamond substrate. The diamond was slightly miscut so that the reflectivity is free of diffraction peaks from diamond. With this setup, they observed a deviation from the reflectivity expected for an interface, in the form of a broad hump peaked at ~1.5 Å^{-1}. The best fit to the data, assuming an exponentially decaying sine density profile, showed an oscillation period of 3.83 Å which corresponds to the distance between two consecutive (001) planes of almost upright Ga_2 dimers in solid α-Ga. The appearance of the α-gallium phase is very suggestive of nucleation induced by the commensurate substrate structure, given that Ga_2 is a small portion of the bulk liquid gallium [11] and that no Ga_2 layering has been observed at the free surface [10]. Moreover, gallium at room temperature (where the experiments were done) is in a supercooled state 8 °C below the freezing point.

More recently, another experiment using x-ray reflectivity [8] has reported a density anomaly in liquid hexane at a solid–liquid interface. Thin hexane films were deposited on silicon substrates from hexane vapor by maintaining a small temperature difference between the substrate and the vapor.

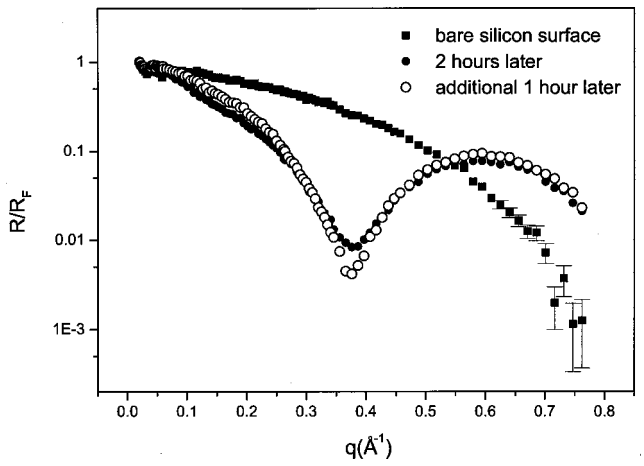

FIG. 1. Reflectivity for cleaned silicon under helium flow immediately after cleaning and drying with nitrogen gas, 2 h later, and an additional 1 h later. Each scan took about 20 min.

The reflectivity data was fitted by one anomalously dense layer 11 Å thick, which does not match the periodicity of 4 to 5 Å seen in surface force experiments on *n*-alkanes [15].

In our own experiments described below, we endeavored to eliminate possible special sources of enhanced ordering, such as crystalline substrates, or the use of supercooled, metallic, liquid crystalline or otherwise exceptional liquids. We present data on interfacial layering in three normal liquids, at temperatures distinctly higher than their freezing points (see details in Sec. II), where any observed ordering must be a general effect of physical confinement by a hard wall.

II. EXPERIMENTAL DETAILS

The (111) silicon substrates ($3\times1\times0.1$ in.) were purchased from Semiconductor Processing, Inc. They were cleaned in a strong oxidizer, 70% sulfuric acid and 30% hydrogen peroxide (70:30 v/v), for 30 min at 90 °C, rinsed 10–15 times with a copious amount of pure water ($>17.5\,\mathrm{M}\Omega$ cm, Nanopure), and stored in water until used.

The x-ray reflectivity curve from uncoated silicon surfaces tends to vary from sample to sample, presumably because of differences in polishing and cleaning procedures and sample chamber conditions. We checked the reflectivity from our cleaned silicon substrates in our sample chamber with helium flowing, i.e., the same conditions as for the liquid film studies to be described below. Figure 1 shows the reflectivity for the bare silicon immediately after cleaning, 2 h later, and 3 h later. These data show that a ~7 Å thick layer of impurities is adsorbed during the first 2 h, but subsequently the layer becomes denser rather than thicker. The trends we see are similar to those shown in Fig. 1 of Ref. [16]. It will be seen that the features of the data from liquid films are quite different from those seen at the silicon-air interface with or without impurities. However, our data do show that ambient impurities can be adsorbed. This will be discussed further below.

To prepare ultrathin liquid films (45–90 Å), we made very dilute solutions of tetrakis(2-ethylhexoxy)silane (TEHOS; see Fig. 2 for the molecular structure) in hexane. We

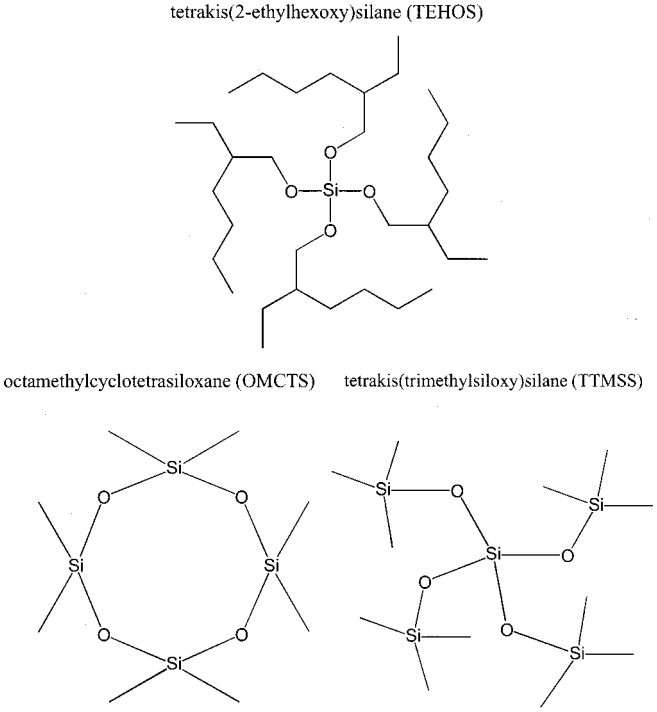

FIG. 2. Molecular structure of TEHOS, OMCTS, and TTMSS.

then dipped the silicon substrates in the solution, and withdrew them at constant speeds to get uniform film thicknesses. The reflectivity measurements were made at least 30 min after deposition; at this point all the hexane had evaporated, leaving only an ultrathin film of nonvolatile TEHOS.

''Thick'' films of TEHOS, octamethylcyclotetrasiloxane (OMCTS), and tetrakis(trimethylsiloxy)silane (TTMSS) shown in Fig. 2 for the molecular structures were prepared simply by pouring them onto silicon substrates and letting the substrate sit vertically until visible interference patterns are seen on the substrate surfaces. This typically takes 40 min to 1 h for TEHOS, and 5 min for OMCTS and TTMSS. Excess liquid was drained with paper tissues at the lower edges of the substrates. The regions studied with x-rays were at least 2 cm away from the draining edge. The film thicknesses are estimated to be 4000–6000 Å. The exact thickness is not important as long as the Kiessig fringes do not appear, because the off-specular background was measured immediately before and after each specular data point. This allowed us to study OMCTS and TTMSS, which evaporate noticeably during the experiment (they evaporate too fast to be studied in the form of ultrathin 45–90 Å films).

X-ray reflectivity studies were performed at beamlines X18A (MATRIX) of the National Synchrotron Light Source and at Sector 10 (MRCAT) of the Advanced Photon Source. The samples were placed under helium during the measurements to reduce background scattering and radiation damage.

III. RESULTS

A. Ultrathin (<100 Å) films

In an earlier paper [12], we determined, using model-independent fitting [17] of x-ray reflectivity data, that the

molecules in 45–90 Å thick TEHOS films were layered close to the solid-liquid interface. We first fitted the data with a ''base model,'' in which the liquid is represented as a slab of uniform electron density with error-function-broadened interfaces. We then divided the film into a series of thin slabs, and allowed the density of each to vary from the uniform ''base'' density. Each slab has a width of approximately $\pi/q_{\max}$, where $q_{\max}$ is the highest q_z reached during the reflectivity scan. We found that it is useful to insert a second set of density slabs between members of the first set, to smooth the electron density profile and get a better fit. When the first set of slabs have been varied to reach the best possible fit, we fixed their densities and fitted the data with the second set of slabs. We then repeated the fit with the first set of slabs while fixing the electron densities of the second set. We will discuss the effectiveness of this procedure later in this paper.

Although the crucial feature of model-independent fitting is the series of density slabs, the ''base model'' plays an essential role. It reduces the computer time required to reach the final fit and leads to a better fit with lower error. The model-independent method can converge on an obviously unphysical electron density profile; the uniform density ''base model'' provides a suitable starting point, thus avoiding this problem.

As an example, reflectivity data for an 87 Å thick film are shown in Fig. 3. (Data from a different sample can be found in Ref. [12].) The dashed line through the data shows the best ''base model'' fit, and the solid line shows the model-independent fit. The density as a function of distance from the interface, obtained from such model-independent fits for TEHOS films of various thicknesses, are shown in Fig. 4. Although the densities are not smooth curves because we have not assumed analytical functions, it can be seen that there is almost always a maximum between 10 and 20 Å and a smaller maximum between 20 and 30 Å. These features are present irrespective of the total film thickness.

The Patterson functions obtained from the reflectivity data are also very useful because they can directly indicate the presence of density fluctuations in the liquid film without model assumptions or fitting procedures. In the Born approximation, the Patterson function, the Fourier transform of the normalized reflectivity, can be written as

$$P(z) \propto \int \frac{\partial \rho(z+s)}{\partial s} \frac{\partial \rho(s)}{\partial s} ds,$$

where $\rho(z)$ is the electron density. In other words, the positions of peaks in $P(z)$ correspond to the distances between regions where the density is changing most rapidly. In order to perform the numerical integration, the data are extrapolated with a Gaussian function (for an error-function-broadened interface) up to 4 Å^{-1} (far beyond the measurable range), to eliminate termination effects which would appear otherwise as periodic oscillations.

For the 87 Å TEHOS film in Fig. 3, the positions of the secondary maxima in the Patterson function (inset) directly reveal an important feature of the density fluctuations in liquid films. The Patterson function (thick solid line) shows

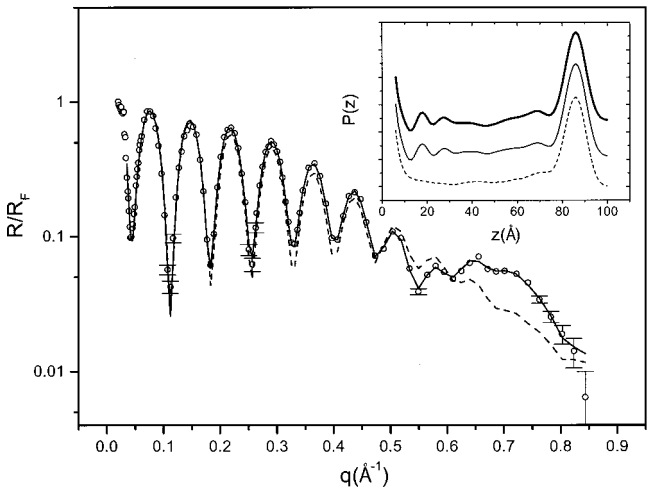

FIG. 3. X-ray reflectivity data from a ~87 Å TEHOS film (open circles); best fit assuming an uniform-electron-density liquid film (dashed line); best fit using a variable (model-independent) electron density within the film (solid line). Inset: Patterson functions, shifted vertically for clarity: from the reflectivity data (bold solid line, top); from the variable-density fit (thin solid line, middle); from the uniform-density fit (dashed line, bottom). The secondary maxima in the 10–30 Å region and the absence of such maxima in the 50–80 Å region indicate that the density fluctuations are closer to the smoother solid–liquid interface. See text for details.

secondary maxima in the 10–30 Å region. The largest $\partial\rho/\partial z$ are at the solid-liquid and liquid-vapor interfaces, and hence the largest peak in the Patterson function is at the film thickness of 87 Å. The smaller maxima at 20 and 30 Å indicate the existence of large $\partial\rho/\partial z$, 20 and 30 Å away from one of the two interfaces. If so, these planes are 57 and 67 Å away from the other interface, and thus there should be corresponding maxima in the Patterson function at these positions. The absence of strong ''symmetric'' features means that one interface is rougher than the other, i.e., has a lower $\partial\rho/\partial z$ than the other, and that the density fluctuations within the liquid are near the smoother interface.

The smoother side can easily be determined from the uniform-density ''base model'' fit. There are only four fitting parameters in this fit (thickness and average electron density of the film and the widths of the two interfaces). The thickness is essentially set by the reflectivity minima, and the average electron density should be about the same as that of the bulk liquid. Unless the average electron density of the liquid is very close to $0.5\rho_{\text{Si}}$ (in our case $\rho_{\text{TEHOS}}=0.43\rho_{\text{Si}}$), the fitting procedure distinguishes the two interface widths unambiguously. We consistently find that the silicon–TEHOS interface is smoother than the TEHOS–air interface. This result, taken together with the peaks in the Patterson functions, tells us that the density oscillations in the TEHOS are near the silicon–TEHOS interface. Of course, this is confirmed by the model-independent fitting.

The open circles in Fig. 5(a) show normalized reflectivity data for a ~57 Å thick TEHOS film taken over a very wide range, up to 1.5 Å^{-1}. The same types of lines as in Fig. 3 are used for the uniform- and model-independent density fits in

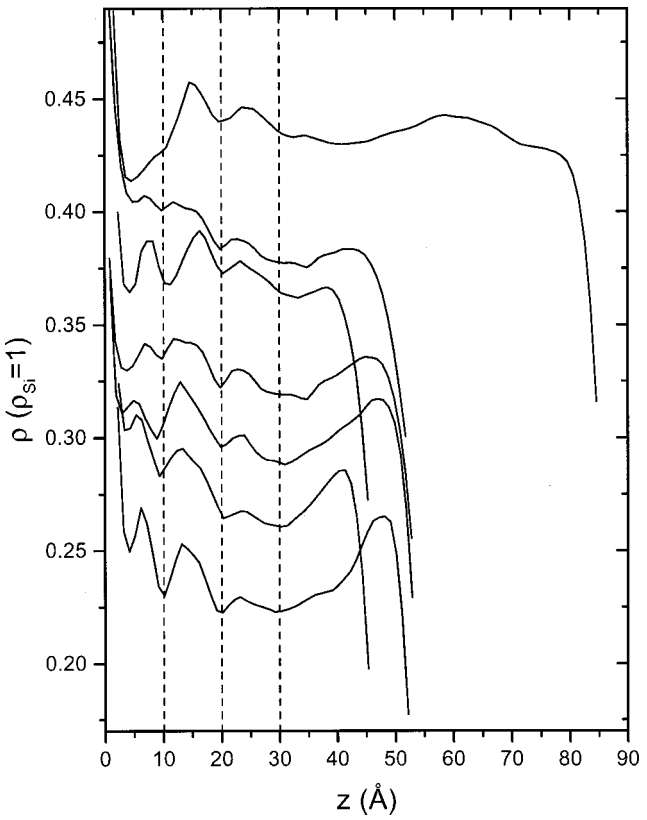

FIG. 4. $\rho(z)$ for various TEHOS samples (thicknesses as marked). Each curve is shifted vertically by $\Delta\rho = 0.013$ from the curve above it for clarity. The second, third, fourth, and fifth curves from the top have been shifted towards the left by small amounts (2, 1, 2, and 1 Å) to bring the minima into approximate registry with the other curves. Taken from Ref. [12], with additional data.

Figs. 5(a) and 5(b). Figure 5(c) shows the electron density profile from the model-independent fit (solid line) with density slabs of 2.5 Å width and the uniform-density fit (dashed line). The density curves obtained without data above 0.9 $Å^{-1}$ are not significantly different, because the high-q data only refine the electron density at smaller length scales.

In summary, the ultrathin film experiments show about three visible internal layers in TEHOS at the liquid-solid interface, with a plane spacing close to the molecule size. We have also seen that the amplitude of the density oscillations decreases as the roughness of the substrate becomes larger [12]. However, although the fitting procedure that we employed is simple and direct, the conclusions derived are not directly obvious from the data. There is a broad hump in the reflectivity, but its identification as a diffraction peak is not very convincing; these data do not show clear diffraction peaks such as those seen due to layering at the free surfaces of liquid metals [9,10]. The density profiles (Fig. 4) are periodic but not very smooth.

On the other hand, Fig. 4 seems to be telling us that the thickness of the film does not matter. If this is so, the layering should exist even at a single interface far from other interfaces, i.e., in a semi-infinite liquid. Such a system would not show the strong reflectivity oscillations (Kiessig fringes)

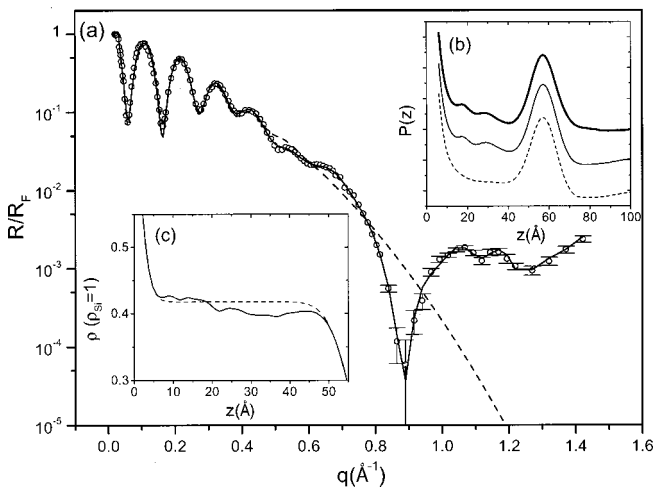

FIG. 5. (a) X-ray reflectivity data from a ~57 Å TEHOS film (open circles); best fit assuming an uniform-electron-density liquid film (dashed line); best fit using a variable (model-independent) electron density within the film (solid line). (b) Patterson functions, shifted vertically for clarity: from the reflectivity data (bold solid line, top); from the variable-density fit (thin solid line, middle); from the uniform-density fit (dashed line, bottom). (c) Calculated electron density: from the uniform-density fit (dashed line); from the variable-density fit (solid line).

visible in the ultrathin film data, and thus allow us to see features of interest much more clearly.

B. Thick films of TEHOS on smooth, rough, and dirty substrates

It has been shown that it is possible to penetrate bulk liquids with higher-energy x-rays for *in situ* studies of chemical processes at interfaces [18,19]. However, the scattering from the bulk liquid is then so strong that it obscures any features in the scattering from the interfacial liquid. We therefore prepared relatively thick films by simply pouring the pure liquid onto the substrate and allowing it to drain until interference patterns on the substrate are visible. The film thicknesses are then estimated to be 4000–6000 Å. Such films are thick enough that there are no Kiessig fringes due to interference between x rays reflected at the solid-liquid and liquid–air interfaces; at the same time, they are thin enough to allow x rays to penetrate without much attenuation and scatter from the interfacial region.

Figure 6 shows reflectivity data for specular and 0.1° off-specular longitudinal scans for ~5000 Å thick TEHOS films [13]. Usually the off-specular ''background'' is subtracted from the specular counts, but we show them separately here to emphasize the similarities and differences. Both scans show peaks at 0.59 $Å^{-1}$, which gives a ''plane spacing'' of 10.7 Å. The small peak in the off-specular data is due to isotropic short-range order in the bulk liquid; its full width at half maximum (FWHM) is 0.25 $Å^{-1}$, corresponding to a coherence length of ~22 Å, about two intermolecular distances. This peak was not affected by silicon surface roughness or cleanliness, confirming that it is due to the bulk liquid. The peak in the specular direction is much stronger, and

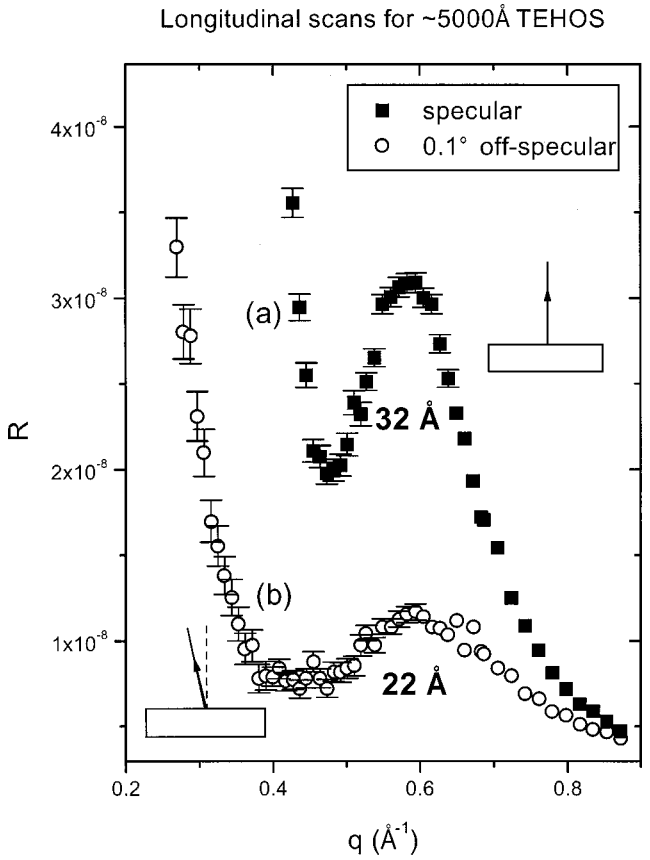

FIG. 6. X-ray scattering from a ~ 0.5 μm liquid film of TEHOS on a clean, smooth (~ 3 Å rms roughness) silicon substrate: (a) wave vector q normal to the substrate surface (i.e., in the specular direction) and (b) same sample but with wave vector q at an angle of 0.1° to the specular direction. The weak peak in the off-specular direction is due to the isotropic correlations in the liquid. The peak in the specular direction is much stronger and slightly sharper; this enhancement is due to layer formation parallel to the silicon surface. From Ref. [13].

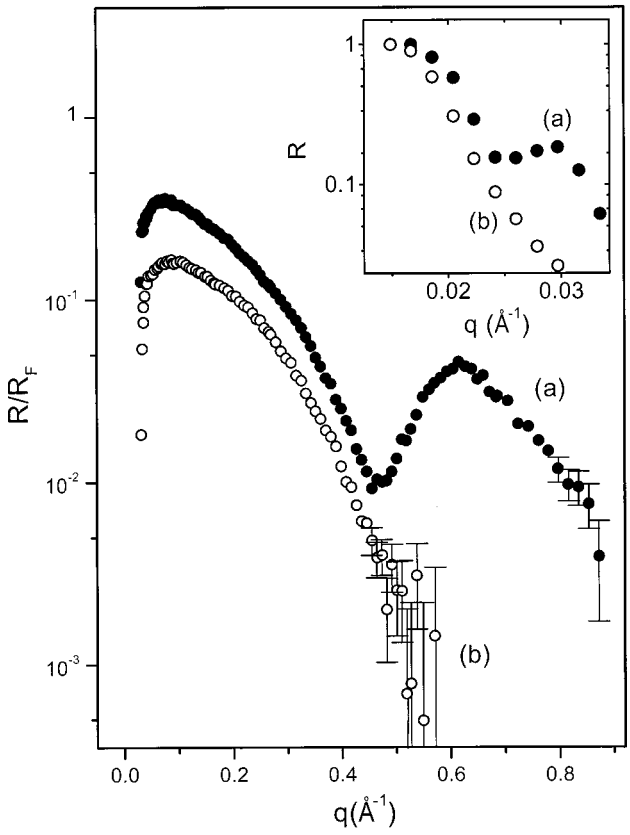

FIG. 7. Normalized reflectivity data for TEHOS from the critical angle (0.0316 Å^{-1}) of silicon: (a) for a film on a clean and smooth silicon substrate and (b) for a liquid film on a clean but visibly rough silicon substrate. The off-specular background has been subtracted from the specular scattering. Inset: Reflectivity data at very low angles. In (a) the two critical angles for reflection at the two interfaces can be seen. In (b) the critical angle for the silicon–liquid interface is not seen because the Si surface is rough, but the liquid–air interface is still smooth enough for the critical angle to be seen. From Ref. [13].

slightly sharper radially (FWHM ~ 0.18 Å^{-1}, corresponding to a coherence length of ~ 32 Å, meaning that there are ~ 3 molecular layers oriented parallel to the substrate surface). Its rocking curve is very sharp (width of $\sim 0.02°$).

Although the data from thick films are visually much more striking than those from ultrathin films, some information is lost. In the ultrathin films, our model-independent fitting placed the layers at the solid-liquid interface because the data contain phase information for reflections from both interfaces as well as from the internal layers. The same information cannot be extracted from the data for thick films. The layers from which the specular peak originates must be in the liquid (the peak is not seen when there is no liquid film), but we cannot tell directly, from the data above, whether the layers are near the solid-liquid or the liquid-air interface. However, we can use a different approach. We prepared similarly thick films, using the same procedures, but on an unpolished (visibly rough) silicon surface. The x-ray reflectivity data are shown in Fig. 7(b). For comparison, Fig. 7(a) is the background-subtracted reflectivity curve, i.e., Fig. 6(a) after subtracting Fig. 6(b). The inset (a) and (b) of Fig. 7 shows the same reflectivities near the critical angle of the silicon substrate. The critical angle for the TEHOS–air interface is seen for both cases at ~ 0.02 Å^{-1}, but only the scattering from the polished surface shows the critical angle of the silicon–TEHOS interface at ~ 0.03 Å^{-1}. (These angles are consistent with those calculated using $\theta_c = \lambda\sqrt{\rho r_0/\pi}$ where r_0 is the classical electron radius. This formula gives $\theta_{c,\mathrm{Si}} = 0.222°$ for $\lambda = 1.5405$ Å [16]. The formula also tells us that $\theta_{c,\mathrm{TEHOS}} = \theta_{c,\mathrm{Si}}\sqrt{\rho_{\mathrm{TEHOS}}/\rho_{\mathrm{Si}}}$ which matches the observations.)

The data in Fig. 7 show that when a rough substrate is used, the liquid–air interface for such a thick film is still as smooth as when a polished substrate is used. However, the specular diffraction peak is not seen with a rough substrate. This tells us that the internal layers in the liquid must be forming near the solid-liquid interface.

The reflectivity in Fig. 7(b) is primarily determined by the surface roughness of the liquid–air interface; the reflection from the rough Si surface is negligible. The absence of Kiessig fringes tells us that the reflections from the two interfaces

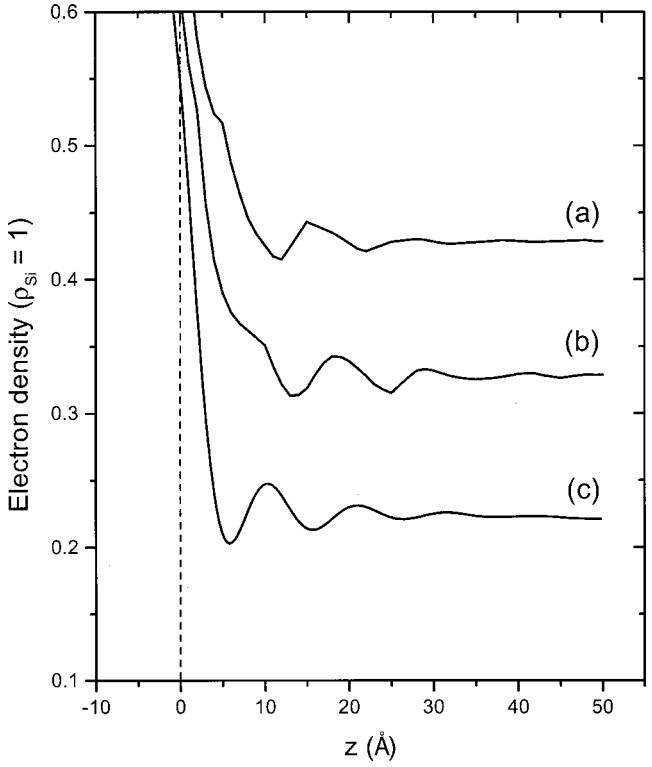

FIG. 8. Electron density profiles resulting from fits to the TEHOS data: (a) from model-independent fitting with one set of slabs (see details in the text); (b) from model-independent fitting with a second set of slabs; and (c) from a fit assuming that there is a decaying sine function density oscillation at the interface. The three curves have been shifted vertically by 0.1 for clarity. Comparing (a) and (b) we find that fitting also with the second slabs smooths the curve (a) and slightly shifts the density oscillations, but does not change the basic conclusions. Very close to the interface, the model-independent fit (b) shows a density that cannot be reproduced by a decaying sine function (c). All three fits give very similar results and demonstrate that the qualitative conclusion (layer formation) is not an artifact of a particular fitting procedure.

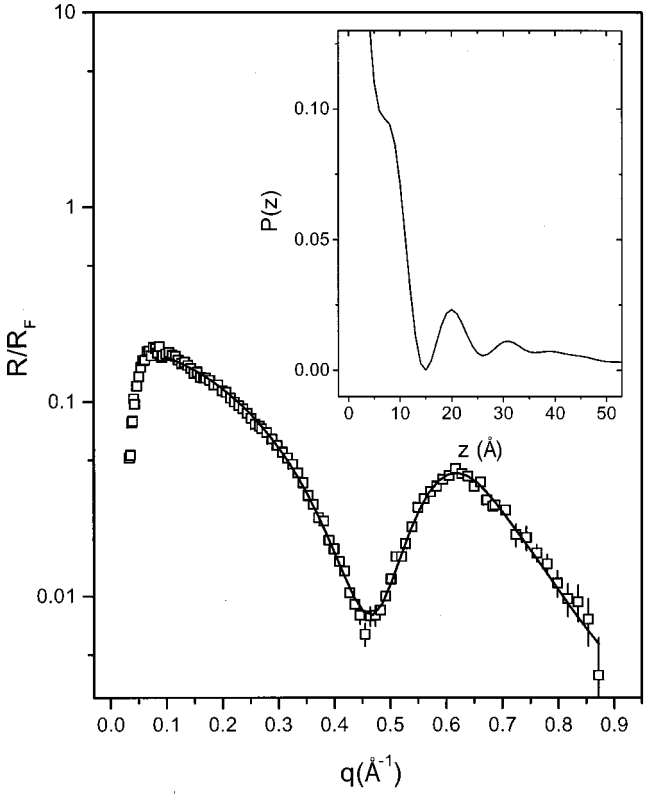

FIG. 9. The normalized reflectivity data for a semi-infinite Si-TEHOS interface, obtained by subtracting Fig. 7(b) from Fig. 7(a). The solid line is a fit using the exponentially decaying sine density model. Inset: corresponding Patterson function for the data (the data below 0.1 Å^{-1} was cut off and extrapolated with a Gaussian curve).

are incoherent; thus the contribution of the liquid-air interface to the smooth substrate data can be removed by simply subtracting the rough substrate data. The difference data can then be treated as the interfacial scattering from a silicon substrate immersed in an infinitely thick liquid. We fitted the difference data using both the model-independent method [Figs. 8(a) and 8(b)] and also separately by assuming that the density variations are an exponentially decaying sine function of the distance from the interface [Fig. 8(c)]. The resulting density profiles are very similar. The difference data are shown in Fig. 9 with the exponentially decaying sine function fit as a solid line. The corresponding Patterson function is shown in the inset of Fig. 9. Further details on fitting are given in Refs. [12,13].

The density profiles in Fig. 8 are shifted down $0.1\rho_{Si}$ for clarity. Figure 8(a) is the best model-independent fit with one set of density slabs; (b) is the best fit with the second (interpolated) set of density slabs. It can be seen that (b) is smoother than (a) and shows clearer $\sim$10 Å density oscillations, although there was only a 2% decrease in the reduced χ^2. The decaying sine function fit (c) shows all the same features, except very close to the interface where a simple analytic function cannot exactly reproduce the behavior revealed by model-independent fits.

We also intentionally contaminated the substrate surface by leaving it in the ambient environment for 5 h after cleaning. We then deposited thick films of pure TEHOS with the usual pouring and draining method. The resulting reflectivity curve is shown in Fig. 10(a). It is clear that the impurities reduce the diffraction peak in the 0.5–0.9 Å^{-1} region compared with Fig. 6(a). However, when the sample is looked at after 8 h without further treatment, the diffraction peak becomes stronger. This is most likely due to the diffusion of impurities into the bulk liquid. These results further confirm that the layering is at the substrate–liquid interface. In Fig. 10(c) we show the reflectivity data for an ultrathin (49 Å) thick film for comparison. The ''hump'' region from 0.5–0.9 Å^{-1} is very similar to that seen with a dirty substrate. This suggests that the ultrathin films are easily contaminated by adsorbed impurities; in contrast to a thick film, it is not possible for impurities in an ultrathin film to diffuse far from the interface region.

C. Thick films of OMCTS and TTMSS

It is reasonable to ask whether the phenomena reported above are unique to TEHOS or a general property of liquids.

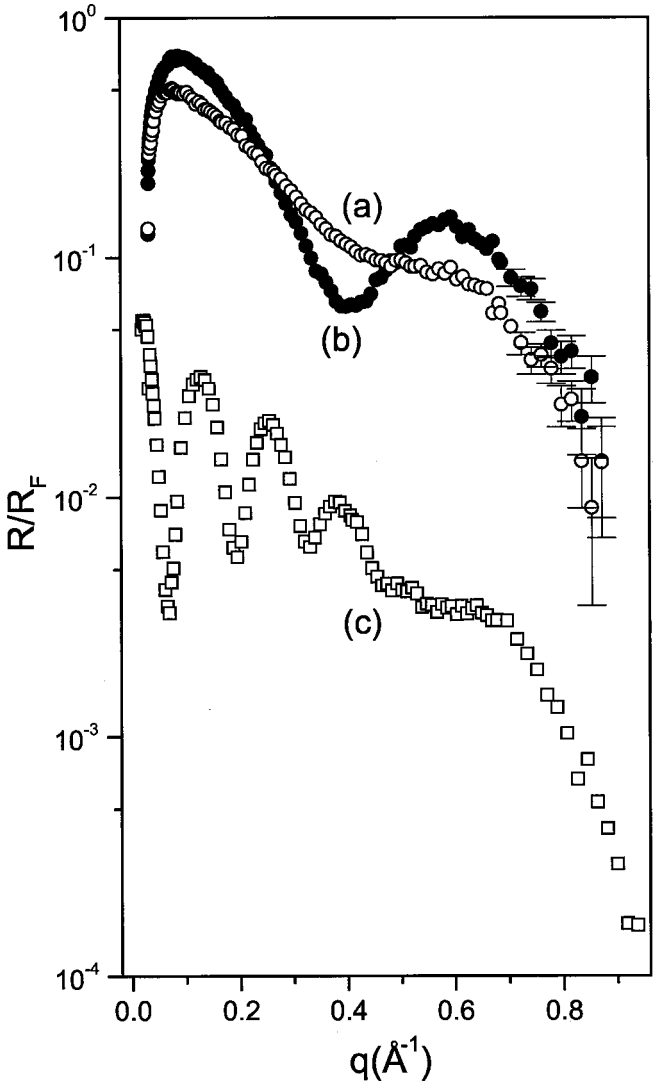

FIG. 10. Normalized reflectivity data for TEHOS films: (a) deposited on a smooth silicon substrate which had been cleaned and then left in air for 5 h and (b) for the same sample after 8 h. The reduction of the diffraction peak in the 0.5–0.9 Å region compared to that seen on a clean silicon substrate [Fig. 6(a)] and the recovery of the peak with time indicate that the layering must be near the solid-liquid interface. (c) 49 Å thick film for comparison, from Ref. [12]. The data are shifted down vertically for clarity. See text for details.

We chose the molecular liquids OMCTS and TTMSS; their molecular structures are shown in Fig. 2. OMCTS has been quite heavily studied with the surface force apparatus, and shows prominent force oscillations when the separation between the two mica plates is less than ~10 times the molecular size [20]. Although the evaporation rates of OMCTS and TTMSS are so large that they could not be used to prepare stable ultrathin films, we were able to obtain reproducible reflectivity data for ~5000 Å thick films. Due to the higher evaporation rate, the film thickness changes during a reflectivity scan, but since the off-specular background (which depends on the amount of bulk liquid) was measured immediately before and after each specular point, the background-subtracted data are insensitive to the film thickness.

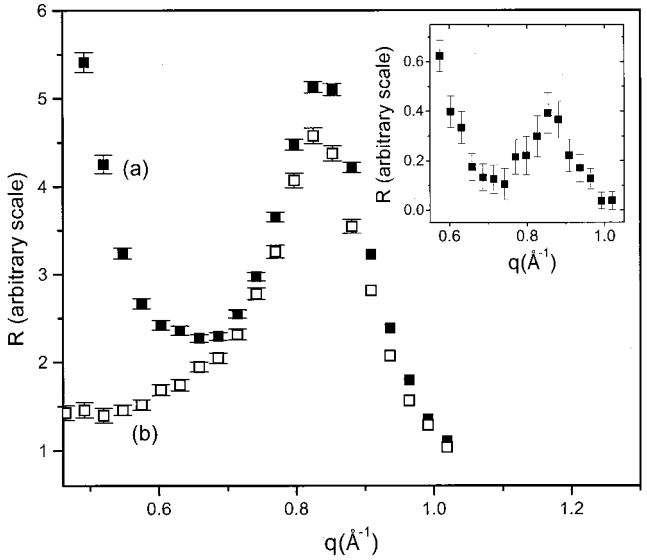

FIG. 11. X-ray scattering with wave vector q in the specular direction (solid squares) and in a 0.1° off-specular direction (open squares), from a ~0.5 μm liquid film of OMCTS on a clean, smooth (~3 Å rms roughness) silicon substrate. Inset: specular reflectivity data after subtracting the background.

The resulting reflectivity curves are shown in Figs. 11 and 12, for OMCTS and TTMSS, respectively. The insets show the background-subtracted specular peaks. Although the OMCTS specular peak is weak, it is statistically significant.

Some bulk and interface spacings and correlation lengths are summarized in Table I. $a=\sqrt[3]{\text{density/weight}}$ is a simple measure of the average bulk spacing. a_b and L_b are average spacing and the correlation length determined from the bulk diffraction peak, and a_s and L_s are the same parameters for

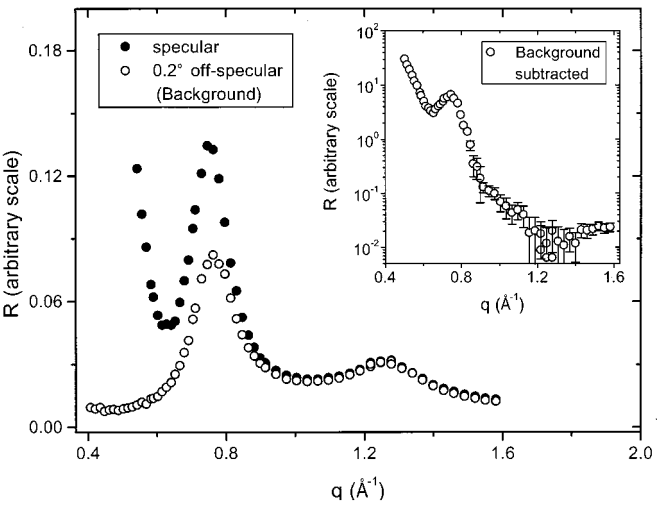

FIG. 12. X-ray scattering with wave vector q in the specular direction (solid squares) and in a 0.1° off-specular direction (open squares), from a ~0.5 μm liquid film of TTMSS on a clean, smooth (~3 Å rms roughness) silicon substrate. Inset: specular reflectivity data after subtracting the background.

TABLE I. Various characteristic lengths for TEHOS, OMCTS, TTMSS, and CCl_4. We notice a similar behavior between TTMSS and CCl_4. (m.p = melting point, T = measuring temperature). See text for other notations.

	m.p(°C)	T(°C)	a(Å)	a_b(Å)	L_b(Å)	L_b/a_b	a_s(Å)	L_s(Å)	L_s/a_s
TEHOS	<-40	25	10.1	10.5	22	~ 2	10.7	32	~ 3
OMCTS	17.4	22	8.0	7.6	33	~ 4	7.3	36	~ 5
TTMSS	-60	0	9.0	8.3	48	~ 5	8.5	55	~ 6
CCl_4	-22.9	25	5.3	4.8	25	~ 5			

the specular diffraction peak after subtracting the background due to the bulk. The ratios L_b/a_b and L_s/a_s express the correlation length as a multiple of the spacing. In all cases, L_s/a_s is larger than L_b/a_b. Both L_b/a_b and L_s/a_s are larger for TTMSS and OMCTS than for TEHOS, but such numbers are not unusual; as shown in Table I, bulk CCl_4 has similarly long correlations [21].

D. Summary

Layering is seen at solid–liquid interfaces using three liquids whose molecules are nonpolar, nearly spherical, nonreactive, non-liquid-crystalline, and well above the melting point. Thus this layering can reasonably be expected to be a general property of liquids. Moreover, we have shown that it occurs at a single liquid-solid interface, not just in an ultrathin film between two proximate interfaces.

ACKNOWLEDGMENTS

This research was supported by the National Science Foundation under Grant No. DMR-9978597. It was performed in part at Beam Line X-18A (MATRIX) of the National Synchrotron Light Source and at Sector 10 (MRCAT) of the Advanced Photon Source; both beam lines and both synchrotron facilities are supported by the U.S. Department of Energy.

[1] B. Bhushan, J.N. Israelachvili, and U. Landman, Nature (London) **374**, 607 (1995).
[2] J. Israelachvili, Acc. Chem. Res. **20**, 415 (1987).
[3] F. Heslot, N. Fraysse, and A.M. Cazabat, Nature (London) **338**, 640 (1989).
[4] M.L. Forcada and C. Mathew Mate, Nature (London) **363**, 527 (1993).
[5] J. Klein and E. Kumacheva, J. Chem. Phys. **108**, 6996 (1998).
[6] For a brief review, see J. Israelachvili, P. McGuiggan, M. Gee, A. Homola, M. Robbins, and P. Thompson, J. Phys.: Condens. Matter **2**, SA89 (1990).
[7] D.Y. Chan and R.G. Horn, J. Chem. Phys. **83**, 5311 (1985).
[8] A.K. Doerr, M. Tolan, T. Seydel, and W. Press, Physica B **248**, 263 (1998).
[9] O.M. Magnussen, B.M. Ocko, M.J. Regan, K. Penanen, P.S. Pershan, and M. Deutsch, Phys. Rev. Lett. **74**, 4444 (1995).
[10] M.J. Regan, E.H. Kawamoto, S. Lee, P.S. Pershan, N. Maskil, M. Deutsch, O.M. Magnussen, B.M. Ocko, and L.E. Berman, Phys. Rev. Lett. **75**, 2498 (1995).
[11] W.J. Huisman, J.F. Peters, M.J. Zwanenburg, S.A. de Vries, T.E. Derry, D. Abernathy, and J.F. van der Veen, Nature (London) **390**, 379 (1997).
[12] C.-J. Yu, A.G. Richter, A. Datta, M.K. Durbin, and P. Dutta, Phys. Rev. Lett. **82**, 2326 (1999).
[13] C.-J. Yu, A.G. Richter, J. Kmetko, A. Datta, and P. Dutta, Europhys. Lett. **50**, 487 (2000).
[14] S.A. Rice, J. Non-Cryst. Solids **205-207**, 755 (1996), and references therein.
[15] H.K. Christenson, D.W.R. Gruen, R.G. Horn, and J.N. Israellachvili, J. Chem. Phys. **87**, 1834 (1987).
[16] I.M. Tidswell, B.M. Ocko, P.S. Pershan, S.R. Wasserman, G.M. Whitesides, and J.D. Axe, Phys. Rev. B **41**, 1111 (1990).
[17] M.K. Sanyal, J.K. Basu, A. Datta, and S. Banerjee, Europhys. Lett. **36**, 265 (1996).
[18] Z. Nagy, H. Yoo, and R.M. Yonco, Rev. Sci. Instrum. **65**, 2199 (1994).
[19] A.G. Richter, M.K. Durbin, C.-J. Yu, and P. Dutta, Langmuir **14**, 5980 (1998).
[20] R.G. Horn and J.N. Israelachvili, J. Chem. Phys. **75**, 1400 (1981).
[21] A.H. Narten, M.D. Danford, and H.A. Levy, J. Chem. Phys. **46**, 4875 (1967).